Research Article

Journal of PeptideScience

Received: 12 September 2010 Revised: 14 December 2010 Accepted: 3 January 2011 Published online in Wiley Online Library: 24 February 2011

(wileyonlinelibrary.com) DOI 10.1002/psc.1356

Folding and assembly of TMD 6-related segments of DMT 1 in trifluoroethanol aqueous solution

Shuyan Xiao, Chunyu Wang, Jiantao Li and Fei Li*

Divalent metal-ion transporter 1 (DMT1) belongs to a large class of metal-ion transporters that drive the translocation of a wide range of divalent metal substrates across membranes toward the cytosol with couple of protons. Two highly conserved histidines in the sixth transmembrane domain (TMD6) are essential for metal transport activity in DMT1. In the present study, we determine the high-resolution structures of three 25-residue peptides, corresponding to TMD6 of the wildtype DMT1 (the segment 255–279) and its H267A and H272A mutants, in 30% TFE-d_2 aqueous solution by the combined use of circular dichroism (CD) and NMR spectroscopies. The wildtype peptide forms an 'α-helix-extended segment-α-helix' structure with two helices spanning over Gly258–Ala262 and Met265–Lys277 linked by a hinge at residues Val263–Ile264. The H267A mutation reduces the hinge to one residue (Ile264), while the H272A mutation extends the flexible region of the central part from Val263 to His267. Diffusion-ordered spectroscopy (DOSY) study demonstrates that all the peptides are self-assembly as trimer in 30% TFE-d_2 aqueous solution. The H272A substitution decreases the intermolecular interaction whereas the H267A substitution may enhance the intermolecular interaction. The specific structure of the discontinuous helix and the self-assembly feature of DMT1–TMD6 may be crucial for its biological function. The changes in conformation and intermolecular interaction induced by histidine substitution may be correlated with the deficiency of DMT1 in metal-ion permeation. Copyright © 2011 European Peptide Society and John Wiley & Sons, Ltd.

Keywords: DMT1-TMD6; structure; assembly; NMR

Introduction

Divalent metal-ion transporter 1 (DMT1), also known as Slc11a2/Nramp2/DCT1, is an integral membrane protein expressed in the plasma membrane, as well as early and late endosomes of various cellular types [1]. Cloning of DMT1 cDNAs has shown that alternative splicing and 3′ end processing yield two DMT1 mRNA variants: one splice form, called as DMT1 (+IRE) mRNA, contains an iron-responsive element (IRE) in the 3′-UTR and encodes a 561 amino-acid protein; while the other splice form, designated as DMT1 (−IRE) mRNA, does not contain a classical IRE and encodes a 568 amino-acid protein [2–4]. DMT1 consists of 12 predicted transmembrane segments, 2 putative glycosylation sites and 1 consensus transport motif [1,5]. It plays an important role in the acquisition and recycle of iron in mammalian cells and transports iron from acidified endosomes into cell cytoplasm [6]. Moreover, DMT1 is the only iron transporter known to be important for the uptake of non-heme iron from the diet across the duodenal mucosa and its expression is upregulated by dietary iron deficiency [7,8]. In addition to iron, DMT1 also transports a variety of other DMTs, including Cu^{2+}, Mn^{2+}, Co^{2+}, Zn^{2+}, Cd^{2+}, and to a lesser extent, Ni^{2+} and Pb^{2+}, but not Ca^{2+} and Mg^{2+} [9]. At low extracellular pH (pH_o), it functions as a proton/metal symporter with H^+ binding preceding Fe^{2+} binding [9,10]. However, the coupling is not strict, DMT1 can apparently operate as an H^+ uniporter, that is, an H^+ 'leak' pathway can proceed uncoupled from divalent cation transport by a built-in proton slip, which could protect the organism from too much intake of metal-ions [11]. At neutral or higher pH_o, DMT1 can transport Fe^{2+} independently of H^+, driven by the electrochemical gradient for Fe^{2+} alone [12]. It was demonstrated that the metal-ion transport is also dependent on Cl^- or other small anions (such as NO_3^- or SCN^-) and the metal-ions may be cotransported with Cl^- [11,13].

Histidine often plays important roles in the function of proteins, mainly because of the chemical versatility of its imidazole ring that can either serve as a ligand-binding site donating imidazole nitrogen lone-pair electrons to the unfilled orbitals of the metal or mediate pH-dependent interactions in proteins by reversibly binding a proton within the physiological pH range [14,15]. Two highly conserved histidines were found in the sixth transmembrane domain (TMD6) of the Slc11 family and have been demonstrated to be important for metal and proton uptake and to facilitate proton-dependent interactions [12,16,17]. Both residues are mutation sensitive. Separate substitutions at either or both residues cause loss of function. Surprisingly, inactive His267 and His272 mutants in DMT1–TMD6 could be significantly activated by progressively lowering pH [17]. Furthermore, the substitution of His272 to Ala uncouples Fe^{2+} transport from H^+ flux and extracellular pH [12].

We previously studied the structures of a 25-residue peptide with the sequence of Ac-Gln-Ala-Val-Gly-Ile-Val-Gly-Ala-Val-Ile-Met-Pro-His^{267}-Asn-Met-Tyr-Leu-His^{272}-Ser-Ala-Leu-Val-Lys-Ser-Arg-NH_2, corresponding to the segment 255–279 of DMT1

* *Correspondence to: Fei Li, State Key Laboratory of Supramolecular Structure and Materials, Jilin University, 2699 Qianjin Avenue, Changchun 130012, P. R. China. E-mail: feili@jlu.edu.cn*

State Key Laboratory of Supramolecular Structure and Materials, Jilin University, Changchun 130012, P. R. China

(TMD6), and its substituent of alanine for histidine at either position 267 (H267A) or 272 (H272A) in SDS micelles. We found that the DMT1–TMD6 adopts an 'α-helix-extended segment-α-helix' structure in which two short α-helical stretches are separated by a central flexible linker [18]. In the present work, we further studied the structure of TMD6 peptide in 30% trifluoroethanol (TFE) aqueous solution using circular dichroism (CD) and NMR methods to ascertain if the discontinuous structure is an intrinsic feature of DMT1–TMD6 and if the effects of H267A and H272A substitutions on the peptide structure are comparative in different membrane mimics. We also inspected the effects of H267A and H272A mutations on the peptide structure. Moreover, we probed the aggregates of the three peptides in the same medium. Although more helical coils are generated due to the strong capability of TFE in inducing helical structure, an 'α-helix-extended segment-α-helix' conformation was still observed for the TMD6 peptide in 30% TFE aqueous solution. Similar to the situation of the peptides in SDS micelles, the H267A mutation makes the central part of the peptide more rigid, while the H272A mutation results in the extension of the central flexible segment. The differences in structures of the peptides lead to their differences in intermolecular interactions.

Materials and Methods

Materials

The peptides were synthesized by GL Biochem Ltd (Shanghai, China). The purity of the peptides was estimated by HPLC and mass spectrometry to be above 95%. Deuterated 2, 2, 2-trifluoroethanol (TFE-d_2; 98%) and D_2O (99.8%) were purchased from Cambridge Isotope Laboratories. All chemicals were used as purchased directly without further treatment.

CD Spectra

The CD samples were prepared by diluting the stock solution of peptides, previously dissolved in TFE, with deionized water to obtain total 500 µl 30% TFE/70% H_2O (v/v). The peptide concentrations were determined as 18.92 µM for WT, 20.18 µM for H267A and 16.75 µM for H272A using the micro-bicinchoninic acid (BCA) protein assay reagent kit [19,20]. Far-UV CD spectra were recorded on a Jasco J-810 spectropolarimeter at room temperature. All spectra were collected in a 0.5-mm cell over the wavelength of 260–190 nm with a scan speed of 50 nm/min, resolution of 0.1 nm, bandwidth of 1.0 nm and response time of 0.25 s. Three scans were averaged for each spectrum and the reference spectrum of the respective medium was subtracted. Data were expressed as molar residue ellipticity [θ], which is defined as $[\theta] = \theta/10\,lcn$, here θ is the observed ellipticity in millidegrees, c is the molar concentration of peptide, l is the length of the light path in centimeters and n is the number of amino-acid residues of peptide.

NMR Spectroscopy

All NMR spectra were acquired at 298 K on a Bruker Avance 500 MHz spectrometer with a z-gradient coil and 5-mm triple resonance inverse (TRI) probe. The samples for NMR experiments were prepared by dissolving certain amounts of peptides in 30% TFE-d_2/70% H_2O (v/v) mixture directly to obtain desired peptide concentrations. Two-dimensional nuclear Overhauser effect spectroscopy (NOESY) experiments were performed using a mixing time of 200 ms with 32–72 transients. Total correlation spectroscopy (TOCSY) experiments were performed using mixing time of 100 and 75 ms with 32 transients. Water suppression was achieved using the WATERGATE technique. All spectra were typically acquired with 2048 data points in F2 dimension and 512 data points in F1 dimension. A shifted sine-bell squared window function in both dimensions was applied before the Fourier transformation and a baseline correction was conducted after the Fourier transformation. All spectra were processed using XWINNMR software (version 3.5) and analyzed using SPARKY [21]. All proton chemical shift values were referenced to TSP [sodium salt of 3-(trimethylsilyl)-propionate-2,2,3,3-d_4].

Structure Calculation

Three-dimensional structures of the peptides were calculated with the program CYANA (version 1.0.6) which uses a simulated annealing combined with molecular dynamics simulation in torsion angle space [22]. Distance restraints were obtained by converting NOE peak intensities into distance upper limits. Structure calculations were initiated from 200 conformers with random torsion angle values and the 20 structures with the lowest target functions were further refined by energy minimization with the AMBER7 program [23] under the force field of Cornell *et al*. [24] using a generalized Born solvent model [25]. Evaluation and visualization of the calculated structures were achieved using the PROCHECK-NMR [26] and MOLMOL [27] software, respectively.

DOSY Experiment

Diffusion-ordered spectroscopy (DOSY) spectra were obtained using bipolar pulse pair stimulated echo (BPPSTE) sequence with WATERGATE for water suppression. The diffusion time (Δ) of 50 ms was used. Duration of the pulse-field gradient (δ) was optimized for each sample in order to obtain the residual signal less than 5% at the maximum gradient strength. The pulse-field gradient (g) was incremented in 16 steps ranging from 2 to 95% of the maximum gradient strength in a liner ramp. All measurements were carried out at 298 K and the data were recorded with 8 scans.

The apparent molecular weights of the peptides were estimated using a previous method [28] where the viscosity of 1.447×10^{-3} N s m^{-2} for 30% TFE/70% H_2O solution [29], the partial specific volume of 7.9×10^{-4} m^3 kg^{-1} for solvent molecule (ν_1) [30] and that of 7.6×10^{-4} m^3 kg^{-1} for peptide (ν_2) [31] were used.

Results and Discussion

Structure Characterization by CD

The CD spectra of all the three peptides in 30% TFE aqueous solution display typical α-helical character, two negative minima near 208 and 222 nm and one positive maximum near 192 nm (Figure 1). The helicity of the H267A mutant is similar to that of the WT peptide, while the helicity of the H272A mutant is smaller that of the WT peptide.

Structure Characterization by NMR

The 2D TOCSY and NOESY NMR spectra of these peptides in 30% TFE-d_2 aqueous solution at 298 K were recorded and analyzed. The fingerprint region of 2D NOESY spectra with assignment and NOE

Journal of PeptideScience

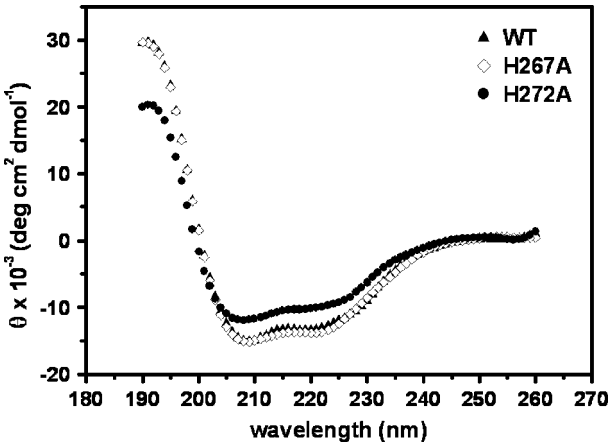

Figure 1. The CD spectra of the WT peptide and H267A and H272A mutants at room temperature.

connectivities along with the Hα chemical shift index (CSI) [32] for these peptides are shown in Figure 2.

For the WT peptide, the strong short-range connectivities H$\alpha(i)$-HN($i+1$), HN(i)-HN($i+1$) and H$\beta(i)$-HN($i+1$) and a large number of medium-range connectivities H$\alpha(i)$-HN($i+3$), H$\alpha(i)$-HN($i+4$), H$\alpha(i)$-H$\beta(i+3)$ and H$\alpha(i)$-H$\beta(i+4)$ from Gly4 to Ser24 are detected (Figure 2A and B). However, there is a shortage of medium-range NOE connectivities H$\alpha(i)$-HN($i+3$) and H$\alpha(i)$-H$\beta(i+3)$ around Ile10, and the CSI values for Val9 and Met11 are $+1$ rather than 0 or -1 like other residues, suggesting a possible change in structure around Ile10 of the peptide. The calculated structure on the basis of the distance constraints from the NOESY spectrum is in good agreement with the predictions from the NOE pattern and CSI criterion. As shown in Figure 3(A), the WT peptide forms a 'α-helix-extended segment-α-helix' conformation in which two short α-helical segments, spanning from Gly4 to Ala8 (corresponding to Gly258 – Ala262 of DMT1) and Met11 to Lys23 (Met265 – Lys277 in DMT1) are separated by a turn composed of residues Val9 and Ile10 (Val263 and Ile264 in DMT1).

In the 2D NOESY spectrum of 2 mM H267A mutant in 30% TFE-d_2 aqueous solution, we found some cross peaks that are clearly not attributed to the intramolecular interactions. When we diluted the sample to the concentration of 0.5 mM, the intermolecular cross-peaks decreased and the chemical shifts of Hα were less changed. Therefore, we determined the structure of the H267A mutant at the concentration of 0.5 mM. The NOESY spectrum demonstrates numerous medium-range NOEs such as H$\alpha(i)$-HN($i+3$), H$\alpha(i)$-HN($i+4$), H$\alpha(i)$-H$\beta(i+3)$ that are diagnostic for an α-helix from Ile5 to Lys23 (Figure 2C and D). However, the CSI data of Ile5 and Val9 – Met11 display an opposite sign from others, implying a possible change in the structure near Ile10. The structure calculation reveals two well-defined α-helices from Ile5 to Val9 (Ile259 – Val263 in DMT1) and Met11 to Val22 (Met265 – Val276 in DMT1) and a turn at residue Ile10 (Ile264 in DMT1) (Figure 3(B)).

For the peptide H272A mutant, most of the medium-range NOE connectivities fall within the region spanning from His13 toward the *C*-terminus with the CSI values of 0 and -1 (Figure 2E and F). The calculated structure displays an α-helix in the *C*-terminal part (over Asn14 – Val22, corresponding to Asn268 – Val276 in DMT1) and a four-residue turn with helical character in the *N*-terminal part (over Ile5 – Ala8, corresponding to Ile259 – Ala262 in DMT1), separated by a flexible linker, as shown in Figure 3(C). The structural statistics of the ensemble of 20 structures with the lowest target function for each peptide is summarized in Table 1. Ramachandran's analyses on the structures of the three peptides indicate that the dihedral angles of all residues involved in the helical spans fall within the allowed regions.

In addition, all proline residues (Pro12) in the three peptides adopt a transconfiguration, as indicated by the cross peaks between the δ-protons of the proline residues and the α-protons of the preceding residues in the NOESY spectra of the three peptides.

Similar to the results in SDS micelles, the TMD6 peptide forms a discontinuous helix structure in the TFE aqueous solution, the H267A mutation decreases the flexibility of the linker and the H272A mutation extends the flexible region of the peptide central part. However, an obvious difference in structures of the peptides was observed, i.e. all helix spans of the peptides in the TFE aqueous solution are longer than those of the peptides in SDS micelles. The difference in structures of the peptides in the two media may arise from following reasons. Firstly, TFE is one of the strongest helix-inducing solvents. Secondly, the peptides in aqueous TFE are self-assembly, which may be stabilized by more coiled – coil interactions. Thirdly, TMD6 contains positively charged histidines. In principle, it is energetically unfavorable to bury these polar residues into the hydrophobic core of membrane. These polar residues may move to the surface of SDS micelles in the absence of interactions with other TMDs, which is unfavorable for the formation of helix. Though the structures of the peptides in solution state are not entirely consistent with those in micelle bound state, the fact that the break of helix is experimentally detected in two different solvents confirms that the discontinuous helix structure may be intrinsic to the sequence.

This characteristic structure of 'α-helix-extended segment-α-helix' has been found in many membrane transporter protein structures and confirmed to be correlated with the transport function [33 – 35]. Coupling and translocation of cations and substrates often involve conformational changes in the hydrophobic interior of the protein. Compared to the α-helix, the extended segment may undergo conformational changes at lower energetic cost. Therefore, the 'α-helix-extended segment-α-helix' structure seems to be prevalent in channels and transporters [36]. Different protein families may share a common transport mechanism where the extended segment in TMD6 would permit the rapid change in structure to accommodate the multifunctional nature of DMT1.

Although the three peptides have similar structures, there are some minor differences. The H267A mutant folds as a long helix with a short and more rigid break in the central part of the structure, while the H272A mutant contains a longer and more flexible central segment consisting of five residues that separates the helices. It is likely that the discontinuous structural nature of this TMD and the length of the extended segment in the central part is crucial for DMT1 folding into the functional form. Given change in structure due to histidine mutation, the TMD may be unable to undergo conformation change as well as the WT peptide does, leading to the loss of activity. Different effects of the two mutations on the structure of the peptide can be explained as follows. There may be certain interactions between backbone atom(s) of His267 and sidechain atom(s) of His272, which favors helix formation. Because H267A substitution does not change the backbone atom(s), the interaction between the two residues can remain. Furthermore, the residue Ala has more helical propensity than His, thus, the structure near position 267 in the H267A peptide has more helical nature than in the WT peptide. However, H272A changes the property of the sidechain of this position, disabling the interaction

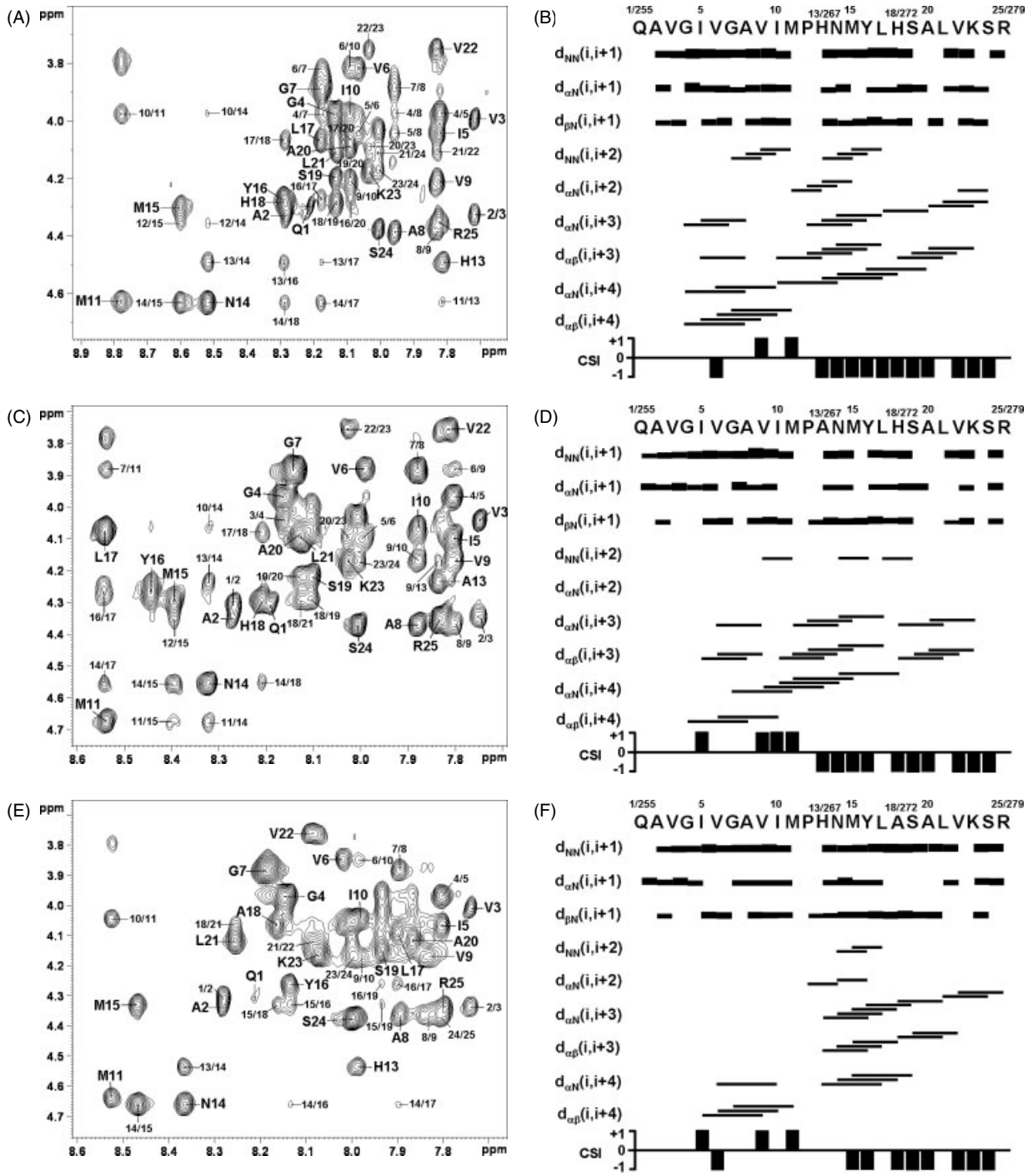

Figure 2. Hα-HN region of 2D NOESY spectra and the NOE connectivities as well as CSI criteria for 2 mM WT peptide (A and B), H267A (C and D) and H272A (E and F) mutants at 298 K.

between the two histidines and thus decreasing helical nature in the proximity of position 267 of the H272A peptide.

Aggregate of the Peptides

Two-dimensional DOSY was used to estimate the aggregate number of the peptides in TFE-d_2 aqueous solution. Nearly identical diffusion coefficients were obtained for the three peptides. The data are 1.019×10^{-10} m^2 s^{-1} for the WT peptide, 1.000×10^{-10} m^2 s^{-1} for the H267A mutant and 1.016×10^{-10} m^2 s^{-1} for the H272A mutant, corresponding to the molecular weights of 6.91, 7.31 and 6.96 kDa, respectively. Therefore, a trimer is assumed for each peptide studied. Diluting the peptide samples from 2 to 0.5 mM (even to 0.25 mM) had little effect on the diffusion coefficients.

We further compare the chemical shifts of Hα and HN of the peptides at the concentration of 2 and 0.5 mM (Figure 4). The Hα chemical shifts of all the three peptides and HN chemical shifts of the WT peptide and H267A mutant are less changed after dilution. However, the dilution results in a remarkable

Journal of PeptideScience

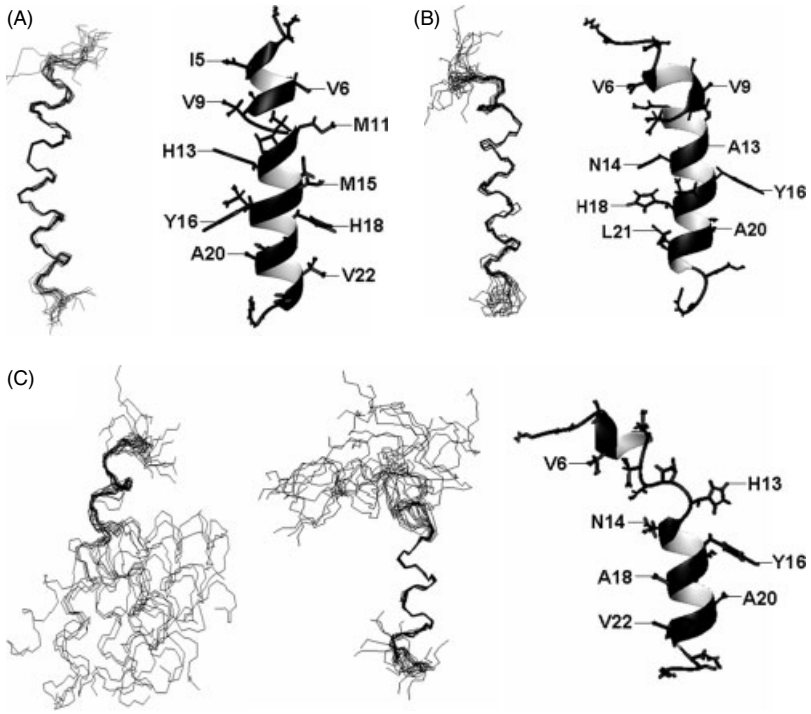

Figure 3. Ensemble of 20 structures with the lowest target functions and ribbon representation for WT peptide (A), H267A mutant (B) and H272A mutant (C, the fitting for the helices in the *N*-terminal and the *C*-terminal regions is displayed, respectively) at 298 K.

Table 1. Structural statistics of the peptides at 298 K

Peptide	WT	H267A	H272A
Average target functions (Å^2)	0.36 ± 0.04	0.20 ± 0.01	0.02 ± 0.01
Number of non-redundant distance restraints	252	232	199
Intraresidual ($\|i-j\|=0$)	89	91	91
Sequential ($\|i-j\|=1$)	87	73	62
Medium ($\|i-j\|\leq 4$)	71	63	40
Long range ($\|i-j\|>4$)	5	5	6
Average sum of distance restraint violations (Å)	2.4 ± 0.2	1.5 ± 0.1	0.1 ± 0.1
Average maximum distance restraint violation (Å)	0.21 ± 0.04	0.18 ± 0.03	0.07 ± 0.04
Average sum of torsion angle restraint violations (°)	0.9 ± 0.7	0.0 ± 0.0	0.0 ± 0.0
Average maximum of torsion angle restraint violation (°)	0.82 ± 0.70	0.0 ± 0.0	0.0 ± 0.0
AMBER energy (kcal mol^{-1})	−822.0 ± 0.6	−815.2 ± 0.5	−818.1 ± 0.5
R.m.s. deviation from the mean structure (Å)			
All residues			
Backbone heavy atoms	1.47 ± 0.55	1.99 ± 0.69	3.38 ± 1.23
All heavy atoms	2.36 ± 0.62	2.71 ± 0.69	4.36 ± 1.33
Well-defined residues[a]			
Backbone heavy atoms	0.32 ± 0.19(*N*)	0.13 ± 0.05(*N*)	0.51 ± 0.33(*N*)
	0.27 ± 0.11(*C*)	0.42 ± 0.30(*C*)	0.34 ± 0.14(*C*)
All heavy atoms	0.54 ± 0.21(*N*)	0.68 ± 0.28(*N*)	0.98 ± 0.40(*N*)
	0.99 ± 0.22(*C*)	0.98 ± 0.34(*C*)	1.22 ± 0.30(*C*)
Ramachandran plot statistics (at each helical span)			
Residues in most favored region (%)	85.3	88.7	88.3
Residues in additionally allowed region (%)	14.7	11.3	11.2
Residues in generously allowed region (%)	0.0	0.0	0.4
Residues in disallowed region (%)	0.0	0.0	0.0

[a] The well-defined residues are 4–8 (*N*) and 11–23 (*C*) for WT peptide, 5–9 (*N*) and 11–22 (*C*) for H267A mutant and 5–8 (*N*) and 14–22 (*C*) for H272A mutant. The '*N*' and '*C*' here represent the *N*-terminal and *C*-terminal, respectively. The concentration of the H267A peptide is 0.5 mM and those of other peptides are 2 mM.

up-field shift of HN resonance of His13 (His267 in protein) and an evident down-field shift of HN resonance of Met11 (Met265 in protein) for the H272A mutant (Figure 4(B)). This implies that HN proton of His13 may be involved in intermolecular interaction with backbone nitrogen atom of Met11 through H-bond. Dissociation of aggregate after dilution could result in breaking of H-bond and thus an up-field shift of His13 HN proton and a down-field shift of Met11 HN proton. In addition, larger down-field shifts of HN protons for Ala18, Leu21 and Val22 (Ala272, Leu275 and Val276 in protein) were also observed for the H272A mutant (Figure 4(B)). The residues Ala18, Leu21 and Val22 are within helical region of the peptide H272A and face the same side of helix. Given that the peptide aggregates by forming helix bundle and these residues are embedded in a polar interior of the helix bundle, the dissociation of the helix bundle would lead to the HN protons of these residues more exposed to solvent, while other residues experience similar environments before and after dissociation. The change in the environmental polarity of HN protons, especially the additional interaction of F atoms of TFE and/or oxygen atoms of water molecules with HN protons of the residues Ala18, Leu21 and Val22 after dilution might cause the down-field shift of these residues. The intermolecular interactions of the WT peptide and H267A mutant are strong and the dissociation of the aggregate with dilution is neglectable, while the association of the H272A mutant is weaker and dilution may lead to the dissociation of considerable aggregate. Because the chemical shifts present in NMR spectra are the weighted average of those of monomer and trimer, the dissociation of aggregate with dilution for the H272A mutant may result in the change in the HN resonances. Despite dissociation, the trimeric aggregates are still the predominant states for the three peptides, as shown by their unchanged diffusion coefficients in the two sample concentrations. On the other hand, the strength of intermolecular interactions of the WT peptide and H267A mutant may be also different. The intermolecular interaction of the H267A mutant may be stronger than those of the WT peptide, since a number of cross peaks belonging to intermolecular interactions are observed in the 2D NOESY spectrum of 0.5 and 2 mM H267A mutant in 30% TFE-d_2 aqueous solution.

Self-assembly occurs widely in ion channels which are correlated with transport function [37–39]. Isolated peptides, containing central parts of the pore region, can form a small and artificial ion channel like the integral protein even in membrane mimics environment [40,41]. The previous study using patch clamp measurements demonstrated that TMD6 was able to form multistate ion channels in the presence of manganese as a physiological substrate of MntH (homolog of DMT1) while the H211A mutant (corresponding to H267A in DMT1) almost loss the ion channel activity [42,43]. Based on the self-assembly data, we hypothesize that the trimerization of the wildtype peptide may be significantly implicated in the divalent cation transport of the integral membrane protein DMT1. The H267A or H272A mutant can also aggregate as trimer in 30% TFE aqueous solution, but the stability of the aggregate changes, which may lead to a change in the size of pore and thus hinder the permeation of divalent metal-ions.

Conclusion

All the three peptides adopt a discontinuous helix structure. The breaking part of the helix structure involves about one to two residues near Ile10 for the WT peptide and H267A mutant and five residues spanning Val9–His13 for H272A mutant. All peptides aggregate into trimer, however, the strength of intermolecular interactions is different, stronger for the H267A mutant and weaker for the H272A mutant. The specific structure and aggregate of TMD6 may play a pivotal role in cation binding and transport.

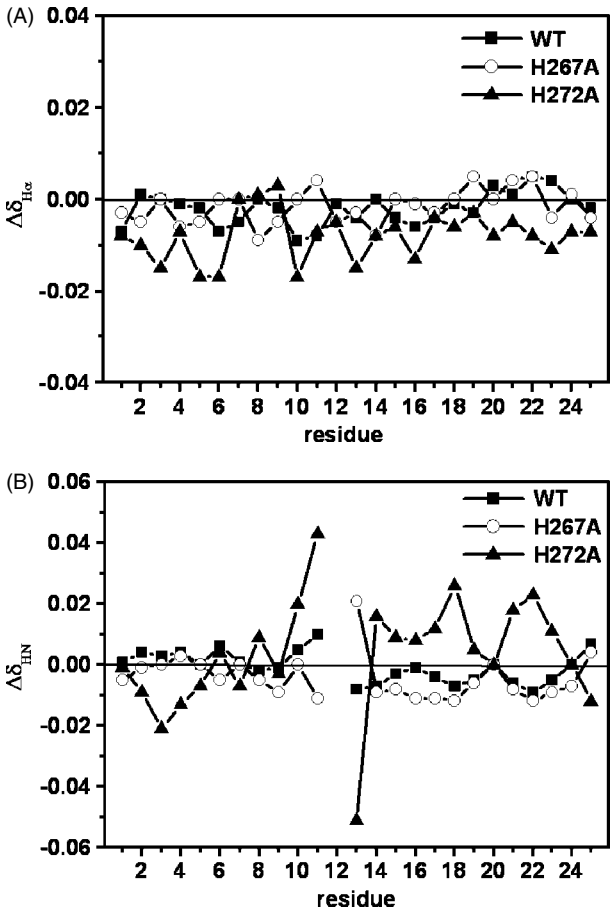

Figure 4. The chemical shifts of Hα (A) and HN (B) of 0.5 mM peptides relative to those of 2 mM peptides at 298 K.

Acknowledgement

This work was financially supported by the NSFC (20973083 and 20934002).

References

1 Gruenheid S, Cellier M, Vidal S, Gros P. Identification and characterization of a second mouse Nramp gene. *Genomics* 1995; **25**: 514–525.
2 Hubert N, Hentze MW. Previously uncharacterized isoforms of divalent metal transporter (DMT)-1: implications for regulation and cellular function. *Proc. Natl. Acad. Sci. U.S.A.* 2002; **99**: 12345–12350.
3 Garrick MD, Dolan KG, Horbinski C, Ghio AJ, Higgins D, Porubcin M, Moore EG, Hainsworth LN, Umbreit JN, Conrad ME, Feng L, Lis A, Roth JA, Singleton S, Garrick LM. DMT1: a mammalian transporter for multiple metals. *Biometals* 2003; **16**: 41–54.
4 Ke Y, Chang YZ, Duan XL, Du JR, Zhu L, Wang K, Yang XD, Ho KP, Qian ZM. Age-dependent and iron-independent expression of two mRNA isoforms of divalent metal transporter 1 in rat brain. *Neurobiol. Aging* 2005; **26**: 739–748.
5 Priwitzerova M, Nie G, Sheftel AD, Pospisilova D, Divoky V, Ponka P. Functional consequences of the human DMT1 (SLC11A2) mutation on protein expression and iron uptake. *Blood* 2005; **106**: 3985–3987.

Journal of PeptideScience

6 Gruenheid S, Gros P. Genetic susceptibility to intracellular infections: Nramp1, macrophage function and divalent cations transport. *Curr. Opin. Microbiol.* 2000; **3**: 43–48.
7 Gunshin H, Fujiwara Y, Custodio AO, Direnzo C, Robine S, Andrews NC. Slc11a2 is required for intestinal iron absorption and erythropoiesis but dispensable in placenta and liver. *J. Clin. Invest.* 2005; **115**: 1258–1266.
8 Canonne-Hergaux F, Levy JE, Fleming MD, Montross LK, Andrews NC, Gros P. Expression of the DMT1 (NRAMP2/DCT1) iron transporter in mice with genetic iron overload disorders. *Blood* 2001; **97**: 1138–1140.
9 Gunshin H, Mackenzie B, Berger UV, Gunshin Y, Romero MF, Boron WF, Nussberger S, Gollan JL, Hediger MA. Cloning and characterization of a mammalian proton-coupled metal-ion transporter. *Nature* 1997; **388**: 482–488.
10 Forbes JR, Gros P. Iron, manganese, and cobalt transport by Nramp1 (Slc11a1) and Nramp2 (Slc11a2) expressed at the plasma membrane. *Blood* 2003; **102**: 1884–1892.
11 Nevo Y, Nelson N. The NRAMP family of metal-ion transporters. *Biochim. Biophys. Acta* 2006; **1763**: 609–620.
12 Mackenzie B, Ujwal ML, Chang MH, Romero MF, Hediger MA. Divalent metal-ion transporter DMT1 mediates both H^+-coupled Fe^{2+} transport and uncoupled fluxes. *Pflugers Arch.* 2006; **451**: 544–558.
13 Nelson N. Metal-ion transporters and homeostasis. *EMBO J.* 1999; **18**: 4361–4371.
14 Eng BH, Guerinot ML, Eide D, Saier MH Jr. Sequence analyses and phylogenetic characterization of the ZIP family of metal ion transport proteins. *J. Membr. Biol.* 1998; **166**: 1–7.
15 Müller-Berger S, Karbach D, Kang D, Aranibar N, Wood PG, Rüterjans H, Passow H. Roles of histidine 752 and glutamate 699 in the pH dependence of mouse band 3 protein-mediated anion transport. *Biochemistry* 1995; **34**: 9325–9332.
16 Courville P, Chaloupka R, Cellier MF. Recent progress in structure-function analyses of Nramp proton-dependent metal-ion transporters. *Biochem. Cell Biol.* 2006; **84**: 960–978.
17 Lam-Yuk-Tseung S, Govoni G, Forbes J, Gros P. Iron transport by Nramp2/DMT1: pH regulation of transport by 2 histidines in transmembrane domain 6. *Blood* 2003; **101**: 3699–3707.
18 Xiao S, Li J, Wang Y, Wang C, Xue R, Wang S, Li F. Identification of an "α-helix-extended segment-α-helix" conformation of the sixth transmembrane domain in DMT1. *Biochim. Biophys. Acta* 2010; **1798**: 1556–1564.
19 Brown RE, Jarvis KL, Hyland KJ. Protein measurement using bicinchoninic acid: elimination of interfering substances. *Anal. Biochem.* 1989; **180**: 136–139.
20 Smith PK, Krohn RI, Hermanson GT, Mallia AK, Gartner FH, Provenzano MD, Fujimoto EK, Goeke NM, Olson BJ, Klenk DC. Measurement of protein using bicinchoninic acid. *Anal. Biochem.* 1985; **150**: 76–85.
21 Goddard TD, Kneller DG. SPARKY 3, University of California, San Francisco.
22 Güntert P, Mumenthaler C, Wüthrich K. Torsion angle dynamics for NMR structure calculation with the new program DYANA. *J. Mol. Biol.* 1997; **273**: 283–298.
23 Pearlman DA, Case DA, Caldwell JW, Ross WS, Cheatham TE III, DeBolt S, Ferguson D, Seibel G, Kollman P. AMBER, a package of computer programs for applying molecular mechanics, normal mode analysis, molecular dynamics and free energy calculations to simulate the structural and energetic properties of molecules. *Comput. Phys. Commun.* 1995; **91**: 1–41.
24 Cornell WD, Cieplak P, Bayly CI, Gould IR, Merz KM, Ferguson DM, Spellmeyer DC, Fox T, Caldwell JW, Kollman PA. A second generation force field for the simulation of proteins, nucleic acids, and organic molecules. *J. Am. Chem. Soc.* 1995; **117**: 5179–5197.
25 Onufriev A, Bashford D, Case DA. Modification of the generalized Born model suitable for macromolecules. *J. Phys. Chem. B* 2000; **104**: 3712–3720.
26 Laskowski RA, Rullmann JA, MacArthur MW, Kaptein R, Thornton JM. AQUA and PROCHECK-NMR: programs for checking the quality of protein structures solved by NMR. *J. Biomol. NMR* 1996; **8**: 477–486.
27 Koradi R, Billeter M, Wüthrich K. MOLMOL: a program for display and analysis of macromolecular structures. *J. Mol. Graphics* 1996; **14**: 51–55.
28 Xiao S, Wang Y, Yang L, Qi H, Wang C, Li F. Study on structure and assembly of the third transmembrane domain of Slc11a1. *J. Pept. Sci.* 2010; **16**: 249–255.
29 Fioroni M, Diaz MD, Burger K, Berger S. Solvation phenomena of a tetrapeptide in water/trifluoroethanol and water/ethanol mixtures: a diffusion NMR, intermolecular NOE, and molecular dynamics study. *J. Am. Chem. Soc.* 2002; **124**: 7737–7744.
30 Minamihonoki T, Ogawa H, Nomuraa H, Murakami S. Thermodynamic properties of binary mixtures of 2,2,2-trifluoroethanol with water or alkanols at $T = 298.15$ K. *Thermochim. Acta* 2007; **459**: 80–86.
31 Perkins SJ. Protein volumes and hydration effects. The calculations of partial specific volumes, neutron scattering matchpoints and 280-nm absorption coefficients for proteins and glycoproteins from amino acid sequences. *Eur. J. Biochem.* 1986; **157**: 169–180.
32 Wishart DS, Sykes BD, Richards FM. The chemical shift index: a fast and simple method for the assignment of protein secondary structure through NMR spectroscopy. *Biochemistry* 1992; **31**: 1647–1651.
33 Yamashita A, Singh SK, Kawate T, Jin Y, Gouaux E. Crystal structure of a bacterial homologue of Na^+/Cl^-dependent neurotransmitter transporters. *Nature* 2005; **437**: 215–223.
34 Weyand S, Shimamura T, Yajima S, Suzuki S, Mirza O, Krusong K, Carpenter EP, Rutherford NG, Hadden JM, O'Reilly J, Ma P, Saidijam M, Patching SG, Hope RJ, Norbertczak HT, Roach PC, Iwata S, Henderson PJ, Cameron AD. Structure and molecular mechanism of a nucleobase-cation-symport-1 family transporter. *Science* 2008; **322**: 709–713.
35 Hunte C, Screpanti E, Venturi M, Rimon A, Padan E, Michel H. Structure of a Na^+/H^+ antiporter and insights into mechanism of action and regulation by pH. *Nature* 2005; **435**: 1197–1202.
36 Screpanti E, Hunte C. Discontinuous membrane helices in transport proteins and their correlation with function. *J. Struct. Biol.* 2007; **159**: 261–267.
37 Chill JH, Louis JM, Miller C, Bax A. NMR study of the tetrameric KcsA potassium channel in detergent micelles. *Protein Sci.* 2006; **15**: 684–698.
38 Carpenter T, Bond PJ, Khalid S, Sansom MS. Self-assembly of a simple membrane protein: coarse-grained molecular dynamics simulations of the influenza M2 channel. *Biophys. J.* 2008; **95**: 3790–3801.
39 Aller SG, Eng ET, De Feo CJ, Unger VM. Eukaryotic CTR copper uptake transporters require two faces of the third transmembrane domain for helix packing, oligomerization, and function. *J. Biol. Chem.* 2004; **279**: 53435–53441.
40 Opella SJ, Marassi FM, Gesell JJ, Valente AP, Kim Y, Oblatt-Montal M, Montal M. Structures of the M2 channel-lining segments from nicotinic acetylcholine and NMDA receptors by NMR spectroscopy. *Nat. Struct. Biol.* 1999; **6**: 374–379.
41 Shindo K, Takahashi H, Shinozaki K, Kami K, Anzai K, Lee S, Aoyagi H, Kirino Y, Shimada I. Solution structure of micelle-bound H5 peptide (427–452): a primary structure corresponding to the pore forming region of the voltage dependent potassium channel. *Biochim. Biophys. Acta* 2001; **1545**: 153–159.
42 Nunuková V, Jelokhani-Niaraki M, Urbánková E, Chaloupka R. Biophysical properties of transmembrane segment 6 of E. coli MntH transporter. *Biophys. J.* 2009; **96**: 327a–327a.
43 Nunuková V, Urbánková E, Jelokhani-Niaraki M, Chaloupka R. Ion channel activity of transmembrane segment 6 Escherichia coli proton-dependent manganese transporter. *Biopolymers* 2010; **93**: 718–726.

